

RESEARCH PAPER

Finite Element Modeling of High Strength Self-Compacting Concrete T-Beams under Flexural Load Reinforced by ARFP

Sinan Abdulkhaleq Yaseen¹ & Muhammad Ali Ihsan²

^{1,2}Department of Civil Engineering, College of Engineering, Salahaddin University-Erbil, Kurdistan Region, Iraq

ABSTRACT:

A finite element models were constructed for comparison self-compacted concrete (SCC) T-beams to study a behavior change of these that reinforced with aramid fiber reinforced polymer (AFRP) and steel bars when compared with experimental data. Nine T-beam specimens reinforced with ARFP and three beams reinforced with steel bars were modeled and analyzed. The key variables were different high strength self-compacted concrete compressive strength, different ratios of AFRP and conventional steel bars for comparison. The comparison for output of flexural strain, load-deflection relationship and crack propagation are taken into consideration. The FE models by using (ANSYS) software show good agreement with the experimental data from previous study by (Yaseen, 2020). The numbers of cracks were reduced in all FE models while the final crack spacing was smaller than experimental samples by maintain the final deflection. Beams reinforced steel bars show better load capacity than those reinforced by AFRP. The FE models were stiffer than the experimental beams. The overall trend of analytical and experimental beam capacity vs reinforcement ratio, shows that the ANSYS response was conservative compared with experimental data of SCC AFRP reinforced beams.

KEY WORDS: FE T-Beam, FEA Method, Flexural behavior, Aramid fiber reinforced polymers, and Self-compacting concrete.

DOI: <http://dx.doi.org/10.21271/ZJPAS.32.6.18>

ZJPAS (2020) , 32(6);176-184

INTRODUCTION:

The precast or cast in-situ reinforced concrete is widely used for constructing structural element. Reinforced concrete T-section beam is one of these elements used in bridge construction, and in most cases the reinforced concrete T-section may be monolithically built in which a part of the slab close to the beam section help in resisting the flexural load. The cast in-situ elements are cast in a prepared molds, so the slab and beams work as monolithic reinforced concrete structure to resist higher load capacities (Ofonime & Ndifreke, 2016; Nabil et al, 2013).

Among several concrete types, Self-compacting concrete (SCC), found to be a special one in its high performance, segregation resistance, excellent deformability and it doesn't need vibration to fill small detailed corners during placing process. The SCC is used instead of conventional concrete when the ongoing properties are needed in casting any structural members (Yasser, 2012; Kamal et al, 2001). Durability of reinforced element has the most point of importance. Using steel bars in bridges, chemical industry buildings and construction near the coastal region causes a corrosion for existing reinforcement bars. Therefore, a need for alternative bars come out to fill the weakness of concrete structure in tension. Aramid fiber reinforced polymers (AFRP), fiber-reinforced polymers (FRP), and glass fiber reinforced polymers (GFRP), are a high-performance reinforcement that have high strength-to-weight ratio and corrosion resistance were used instead of conventional steel bars (Guowei, 2011; Rolland,

* Corresponding Author:

Sinan Abdulkhaleq Yaseen

E-mail: sinan.yaseen@su.edu.krd

Article History:

Received: 23/12/2019

Accepted: 15/08/2020

Published: 20/12/2020

2014). This work is aiming at FE modeling, supported by experimental work, to use it in analyzing the flexural behavior of T-sectioned beam that are constructed by using self-consolidation concrete and ARFP bars, since very little work was found on finite element modeling of the related experimental work. Subramani et al. (Subramani et al, 2017) recorded that ultimate tensile strength, the modulus of elasticity of the used bars and beam width was the most affected parameters by changing the applied load, so the modeling must be controlled. Ofonime and Ndifreke (Ofonime and Ndifreke, 2016) studied the effect of increasing the flange width on beam stiffness, the initial crack load, and the load deflection curve. The beam samples were simulated accurately by using LS DYNA software. Buyukkaragoz et al. (Buyukkaragoz et al., 2013) made a numerical study of concrete beams reinforced with AFRP bars to focus on the flexural behavior. The loads on the beams found by FE analysis were close to those from the effective moment of inertia expressions, and the numerical ultimate moments also correlated well with the analytical values of concrete stress-strain models. Numerical analyses, which hardly predict the sudden reduction in the flexural rigidity of FRP-reinforced concrete beams due to the crushing of cover concrete, were shown to provide somewhat conservative deflection estimates. Yaseen (Yaseen, 2020) experimentally investigated the flexural behavior of T-beams made by self-compacting concrete and reinforced with ARFP.

In this study, a total of 9 T-sectioned beams were modeled to see the agreement of FE model beams with experimental data for beams having the same properties and same loading condition (ACI 440.1R, 2006). The material definitions were made for SCC to work as a matrix and ARFP reinforced bars to work as a fiber in the simulation of these T-beams.

The paper objective is to use FE model for estimation an accurate stresses and to see the response of structural components (having slab-beam action) when used in long span members, bridges and other similar applications. Constructing FE models to compare with an experimental data from Yaseen's study (Yaseen, 2020), for find behavior change in flexural using p-delta curve, mode of failure, and crack pattern, due to change in SCC strength and reinforcement

ratio using ARFP bars. A simulation of simply supported SCC T-beams, covering significant key variables, and loaded by static loading is made using ANSYS 18 program (ANSYS, 2018; Srinivasan & Sathiya, 2010).

1. FINITE ELEMENT MODEL SIMULATION

As mentioned previously, the ANSYS computer program was used to analyze all the tested beams, the FE analysis of these models is not dedicated for T-Beam SCC casted models which have the same hardened property as a normal concrete to conform the T-Beam SCC casted

experimental results. ANSYS has a ability to build a finite element model and simulate the actual boundary condition of the beam elements. The finite element technique is used to simulate the behavior of self-compacted concrete T-beams reinforced with AFRP bars. The matrix and fiber definition were utilized to construct the FEM. These models were the integration of the three phases of finite element analysis that involve defining the model, boundary conditions and loadings, then the preprocessing, solution, and post-processing.

1.1. AFRP Reinforced Concrete Element Definition

The material and element specification of AFRP reinforced Concrete must be defined in any used modeling software to be able to show the interaction between concrete and reinforcement and represent concrete cracking, and crushing. The width reduction of crack growth and the ability of transferring flexural stress after first crack occurs can be found by the interaction between concrete and reinforcement. An eight-node three-dimensional solid element is used to represent the AFRP Reinforced Concrete, called (Solid65) Fig. (1). Each node had three degrees of freedom (u, v, and w, in three direction x, y, and z respectively). The element has ability of plastic deformation and is used to investigate failures in flexural deficit beams.

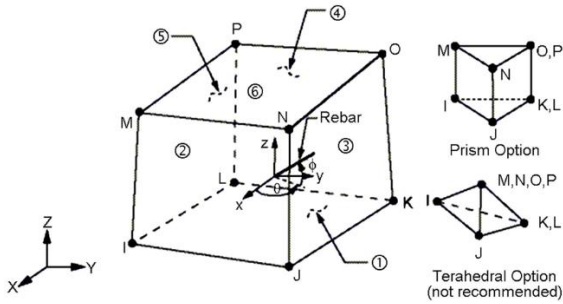


Figure 1: Three-dimensional eight-node solid element

1.2. AFRP and steel Stirrup Reinforcement Modeling

The definition of AFRP and stirrup steel bar with their property, can actualize in finite element method by techniques called, discrete, embedded, and smeared representations Fig. (2). A two-node individual representation of main flexural bars (AFRP bars) and shear reinforcement (steel bars) were modeled using 3-D spar elements (Link180), which allow the elastic–plastic response of reinforcing bars (ANSYS, 2011). It is merged with 8 nodal element that represent the reinforced concrete. Some assumptions taken in to consideration, the perfect bond between the nodes of (AFRP and Steel) bars elements and the corresponding nodes for the concrete elements, and the two type of bars carry axial load only.

The difference between the material properties (concrete, AFRP, steel bars) lead to necessities of connecting these distinct elements to allow for the best transforming the load, stresses and strains among them. It means that they share the same nodes. The actual stress–strain curve adopted from the tensile tests is used to determine stress–strain relationship of all type of reinforcement.

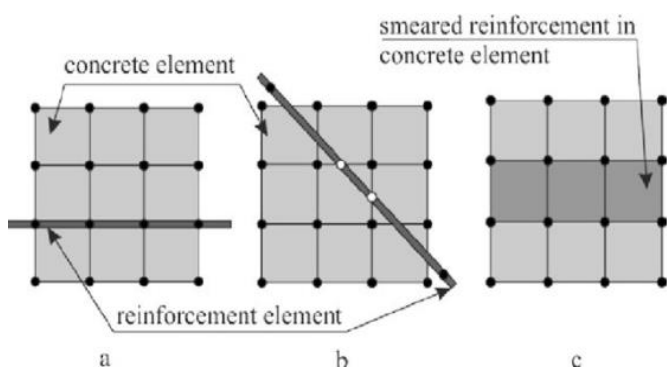


Figure 2: Reinforced concrete model representations (a) Discrete; (b) Embedded; and (c) Smeared

1.3. Load transferring bearing plates

A bearing plate is needed under load point connection with the beams. To prevent any stress accumulation at certain points, 10 mm-thick

plates were placed under two points (third-point loading test). This will reduce and distribute the stress to prevent crushing near the supporting point. Solid 185 elements were used to identify the base plate (ANSYS, 2018).

2. MATERIAL PROPERTIES MODELLING

2.1. Self-compacted Concrete Modeling

Concrete is a quasi-brittle material with different compression and tension behaviors. It is assumed to be homogeneous and initially isotropic. The compressive uniaxial stress–strain relationship for the concrete model is given by Fig.3

The behavior of normal concrete under compression is illustrated in a typical uniaxial stress-strain curve, as shown in Fig. 3, and consists of two parts, linear and nonlinear. The limit of the linear portion is defined as 30% of the maximum compressive strength, the modulus of elasticity (E_c) and Poisson’s ratio (calculated from the linear portion). The nonlinear elastic behaviors of concrete can be defined by the multi-linear stress-strain relationships, as illustrated in Fig. 3.

Used material properties are described below:

Two material models were given: material 1 for concrete, material 2 for AFRP, material 3 for steel, under the linear isotropic material definition.

a) Self compacted concrete with varied strengths:

$$\hat{f}_c = 60 \text{ MPa}, \hat{f}_c = 80 \text{ MPa}, \hat{f}_c = 100 \text{ MPa}.$$

Modulus of elasticity, $E_c = 42.49 \text{ GPa}$, Ultimate Strain = 0.003, Poisson’s ratio, $\nu = 0.2$.

b) AFRP bars:

Modulus of elasticity, $E_a = 50 \text{ GPa}$, $f_u = 1200 \text{ MPa}$, Ultimate Strain = 0.023, Poisson’s ratio, $\nu = 0.28$.

c) Steel bars

Modulus of elasticity, $E_s = 200 \text{ GPa}$, $f_y = 420 \text{ MPa}$, yield Strain = 0.002, Poisson’s ratio, $\nu = 0.30$.

the self-compacted concrete mix proportion and the fresh test results are shown in Table (1) and (2).

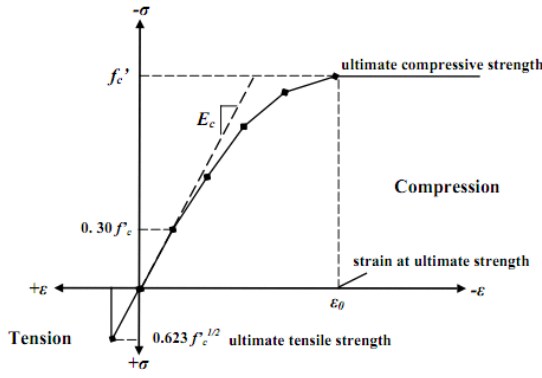


Figure 3: compressive uniaxial stress – strain curve of concrete (ACI, 2016b)

Table (1) Self-compacted concrete mix proportion

Mix No.	Cement kg/m3	Gravel kg/m3	Sand kg/m3	Silica Fume kg/m3	Stone Powder kg/m3	%Super plasticizer By weight of cement	Free water kg/m3	SCC strength at 28 day \hat{f}_c (MPa)
Mix 1	380	850	900	38	57	1.40	155	60
Mix 2	440	800	900	44	66	1.20	165	80
Mix 3	480	900	720	48	72	2.10	139	100

Table (2) Fresh self-compacted concrete test results

Mix No.	Slump Flow (mm)	T ₅₀ (sec)	V-Funnel (sec)	L-Box (H1/H2)
Mix 1	645	4.45	9.65	0.88
Mix 2	675	3.12	8.4	0.91
Mix 3	565	6.85	12.32	0.8

2.2. Geometrical Detail of T-beams

The 12 casted beams were of length 1100mm, over all height 200mm, flange width 200 mm, flange thickness 50mm and web thickness 75mm. (effective depth $d=176.3$ mm). The beams were simple supported and loaded statically under universal loading machine. The test program includes fabrication of T-beams with three different compressive strengths of self-compacted concrete 60, 80, and 100 MPa, and using AFRP as main longitudinal reinforcement with different reinforcements ratios (less than ρ_{bFRP} , between balance and $1.4\rho_{bFRP}$ ratio, and more than $1.4\rho_{bFRP}$).

Also, three beams were casted using conventional steel bars with normal steel balanced reinforcement ratio (ρ_b) to be compared with FE model sample defined by normal steel bar, as a reference. Fig. 4 and Table (3 & 4) present the properties and details of the tested specimens (Yaseen, 2018). Half of the full beam was used for modeling by taking advantage of the symmetry of the beams. This approach reduced computational time and computer disk space requirements significantly.

Table (3) Tested beam Detail

G. No.	Sample	SCC strength \hat{f}_c (MPa)	Rein.Ratio ρ	No. of main bars	Stirrups	Details
1	TS-11	60	0.83	2-Ø8mm	Ø5.5@75 mm	ρ_b
	TA-12		0.55	1-Ø5mm		$\rho < \rho_b$
	TA-13		1.09	2-Ø5mm		$\rho_b < \rho < 1.4\rho_b$
	TA-14		1.64	3-Ø5mm		$\rho > 1.4\rho_b$
2	TS-21	80	0.97	2-Ø10mm	Ø5.5@75 mm	ρ_b
	TA-22		0.82	2-Ø5mm		$\rho < \rho_b$
	TA-23		1.23	3-Ø5mm		$\rho_b < \rho < 1.4\rho_b$
	TA-24		1.64	4-Ø5mm		$\rho > 1.4\rho_b$
3	TS-31	100	0.78	2-Ø10mm	Ø5.5@75 mm	ρ_b
	TA-32		0.66	3-Ø5mm		$\rho < \rho_b$
	TA-33		1.31	4-Ø5mm		$\rho_b < \rho < 1.4\rho_b$
	TA-34		1.64	5-Ø5mm		$\rho > 1.4\rho_b$

Table (4) Tested Beam Detail

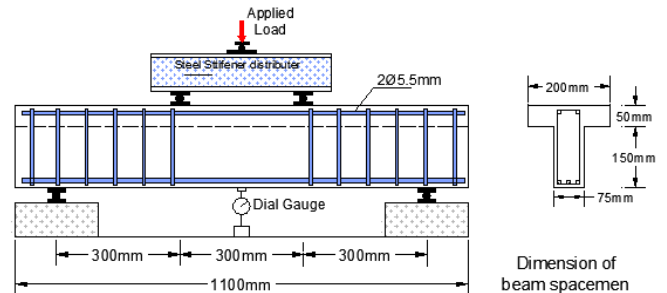
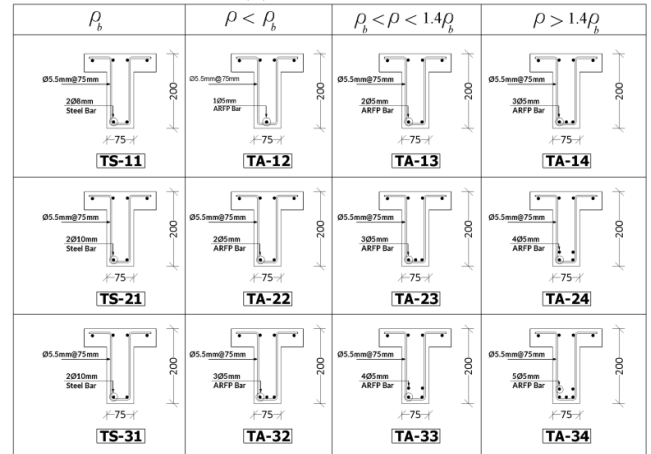


Figure 4: T-Beam geometrical detail with loading

3. LOADING AND BOUNDARY CONDITION

The symmetry allows the use of only half of the beam instead of full sample. A simple supported beam boundary condition was entered. The direction perpendicular to the plane of symmetry must be restrained against displacement. A base plate placed under point load position to prevent the accumulation of stress and it was defined as

steel material with elastic properties. The perfect merge between the nodes is checked to gain the fully interaction between the three material (concrete, AFRP, and steel). In the contact definition, concrete is specified as the master surface while the steel plate is the slave surface. All top nodes of the steel plate at the loading point are pushed down following a prescribed time-displacement curve while ensuring that dynamic effect is negligible, to mimic a quasi-static loading. Figs. 5 & 6 show the one-half finite element model of the reinforced concrete T-beam with reinforcement detail.

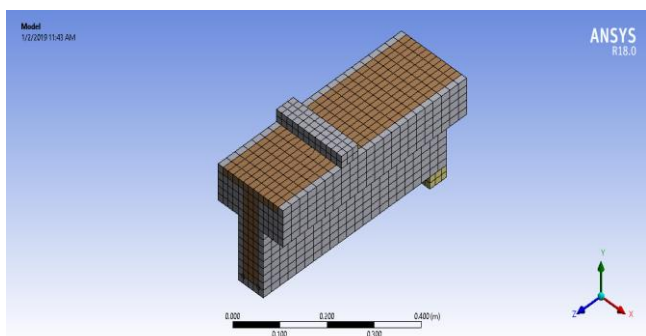


Figure 5: Typical steel reinforcement locations for the half-size beams

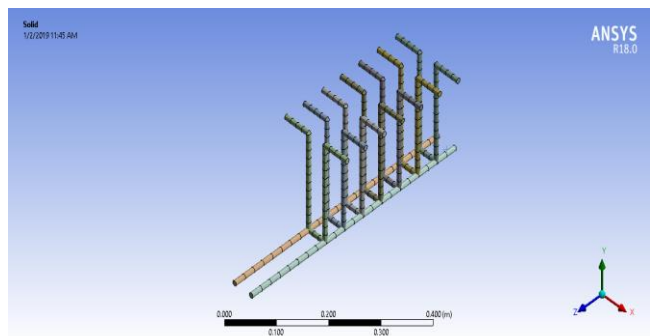


Figure 6: Reinforcement locations for the half-size beams

4. PREDICTED RESULTS FROM THE FINITE ELEMENT MODEL (FEM)

The results of all specimens with their 1st cracking load (The first cracking load from the finite element analysis is the load step where the first signs of cracking occur in concrete elements (solid65)), deflection, ultimate load (ultimate load is the last converge load step P_u), and their final deflections are summarized in Table 5.

4.1. First Cracking Load

A behavior recording of all loading steps is taken by ANSYS. Cracking became visible on the sides of the FE Modeled beam at 12-18% of the failure

Sp.No.	G.No.	Samples	SCC strength $f'c$ (MPa)	Experimental Result				Mode of Failure
				First Crack load kN	Deflection at first crack mm	Failure load kN	Deflection mm	
1	G1	TS-11	60	21.07	1.4	52.67	5.99	Compression
2		TA-12		7	3.17	33.6	79.11	Tension
3		TA-13		8.64	5.9	60.45	87.26	Compression
4		TA-14		9.82	6.2	70.7	91.61	Compression
5	G2	TS-21	80	22.69	0.91	75.64	5.96	Compression
6		TA-22		4.76	2.9	65.03	80.55	Tension
7		TA-23		6.86	3.8	84.38	83.06	Compression
8		TA-24		10.16	5.27	94	89.15	Compression
9	G3	TS-31	100	23.47	0.91	78.25	5.03	Compression
10		TA-32		8.08	1.22	95.35	81.98	Tension
11		TA-33		9.13	3.2	107.57	85.19	Compression
12		TA-34		9.37	3.53	119.93	91.2	Compression

Sp.No.	G.No.	Samples	SCC strength $f'c$ (MPa)	FE Model Result				Mode of Failure
				First Crack load kN	Deflection at first crack mm	Failure load kN	Deflection mm	
1	G1	TS-11	60	19.66	1.2	55.3	6.13	Compression
2		TA-12		6.55	2.78	35.1	79.68	Tension
3		TA-13		8.14	5.6	62.3	87.48	Compression
4		TA-14		9.23	5.82	72.5	91.23	Compression
5	G2	TS-21	80	20.03	0.61	78.3	6.32	Compression
6		TA-22		4.12	2.62	67.3	80.66	Tension
7		TA-23		6.22	2.65	86.2	82.47	Compression
8		TA-24		9.16	5.22	96.12	91.35	Compression
9	G3	TS-31	100	22.12	0.73	80.71	6.51	Compression
10		TA-32		7.89	1.02	97.61	82.12	Tension
11		TA-33		8.99	3.09	119.65	85.24	Compression
12		TA-34		9.07	3.23	128.32	91.78	Compression

load in beams of 60 MPa strength and 6-9% in beams of 80 and 100 MPa strength, while these ratios were a bit larger in experimental data. The first sign cracks were flexural crack occurred at mid-span length of the T-beam specimens, starting at the bottom when the applied load reached the loads shown in result table. The flexural failing pattern seen in all beams. The number of cracks from the ANSYS-FEM analysis is smaller than that observed in the experimental test, see Fig. 7. No more than three cracks can be predicted in each Solid65 element for the FEM. Therefore, the number of cracks shown is affected by the size of the mesh. Using a large mesh size for Solid65 elements would result in few elements and minimal cracks, whereas using a small mesh size would result in the opposite conditions.

The overall first crack load was larger in Finite element model compared with the experimental data. This is due the compatibility between the material definitions making an enhancement in load transferring between the materials and that the cracking load in the experimental test was the load at which the first visible flexural crack appeared, whereas the theoretical cracking load is the load step in which one of the principal stresses in the concrete element reached the maximum limit. The specimens reinforced with steel need very larger loads to reach the first crack when compared with AFRP reinforced samples. Increasing SCC strength from 60 to 100 MPa led to increase the first crack load in same groups of reinforcement ratios.

Table (5) FE model and experimental testing results

The final deflections of AFRP beam were ranged between 79-92 mm, while the deflection in the corresponding beams reinforced with steel were 6-7 mm. The final crack spacing was smaller than experimental samples, mainly because of assuming SCC to be a homogenous isotropic material in FE model which's make the load of first crack be less and the number and crack opening less than experimental. The corresponding strain intensity for the beam sample shown in Fig. 8.

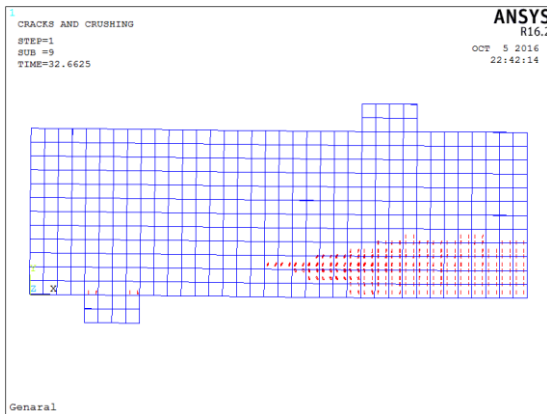


Figure 7: Flexural crack pattern for T-beam

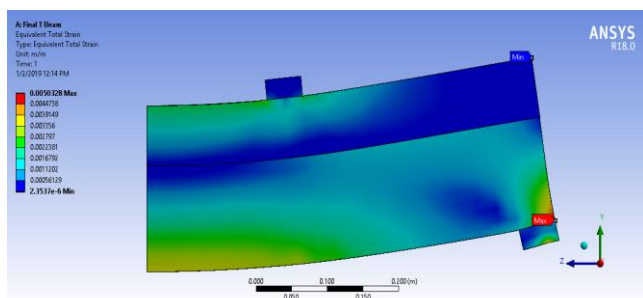


Figure 8: Strain intensity for beam sample by ANSYS

4.2. Compressive Strength Effects on Ultimate Capacity

The influence of self-compacted concrete can be seen for the same reinforcement ratio groups. A small increase of ultimate load capacity is seen for $\rho < \rho_b$ of AFRP ratio, while a larger load carrying capacity is seen for, $\rho_b < \rho < 1.4\rho_b$ and $\rho > 1.4\rho_b$ of AFRP ratio when the strength changed from 60MPa, to 80MPa, and then to 100MPa, Table 1. The T-beams reinforced with steel bars were stiffer by carrying more load when compared with AFRP reinforced beams. The ultimate load capacity of the steel reinforced beam differs by 57.54%, 16.34%, and -17.31% than aramid reinforced beams for same group of concrete strength. These ratios are seen to be more than the experimental data by 0.84%, 1.01%, and 0.65% respectively. This increase in results is occurred because that the concrete was taken as

homogenous material, so more interlocking between the meshes and higher results are occurred. Ultimate load capacity is increased by 41.60% for steel reinforced beams when strength increased from 60MPa to 80MPa. However, ultimate load capacity is increased by 3.07% when strength increased from 80MPa to 100MPa which shows that the effect of strength change is more in low strengths. These ratios coincide with those of the experimental data.

4.3. AFRP Reinforcement Ratio Effect

The change in reinforcing ratio effect for the same strength group made an improvement in ultimate load capacity. The enhancement found to be 77.49%, 28.08%, and 22.57% for 60, 80, and 100MPa strength groups when the ratio increased from $\rho < \rho_b$ to $\rho_b < \rho < 1.4\rho_b$, and the increases were 16.37%, 11.5%, and 7.24% for 60, 80, and 100MPa strength groups when the ratio increased from $\rho_b < \rho < 1.4\rho_b$ to $\rho > 1.4\rho_b$ as shown in Fig. 9. The predicted load of ANSYS model versus the experimental beam data shows a convergence to be ranged from 97-99% for small reinforcement ratios $\rho < \rho_b$ to $\rho_b < \rho < 1.4\rho_b$ and 90% for larger ratios ($\rho_b < \rho < 1.4\rho_b$ to $\rho > 1.4\rho_b$), this is thereby an indication of perfect calibration of FEM model to perform the simulations close to reality.

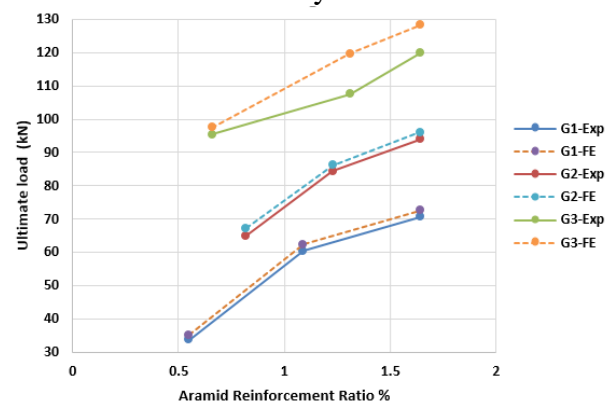


Figure 9: FE model and experimental beam capacity vs. reinforcement ratio

4.4. Load Displacement Relations

The loading stages with the corresponding displacement were recorded. Because of putting displacement transducer at mid span of the experimental tested beam, so the deflections were taken in the same location in FE model at the bottom of the mid span as indicated in Fig. 10. The load-deflection comparison curves of FE models and experimental tested beams are presented in Fig. 11, 12, and 13, for 60-, 80-, and

100-MPa self-compacted concrete respectively. The FE model ultimate load capacity shows slight increase in deflection with respect to the experimental data for all strengths and AFRP ratios. This is an indication of agreement of the constructed model with the experimental beams. The number of cracks were reduced in all FE models. The models were stiffer than the experimental beams because of the non-consideration of the micro-cracks in concrete (because of drying shrinkage), the bond slip of the reinforcement and the assumed perfect bond between the concrete and the reinforcement bar in the FE model, which may not be true for actual beams. The first cracking loads obtained from the ANSYS-FEM is lower than those from the experimental results in the pre-cracking stages. The low modulus of elasticity of AFRP bars made their effect of changing reinforcement ratio be small on reducing the beam mid-span deflection. The deflection of T-beams with steel bars were much smaller than the AFRP reinforced beam, and having more ultimate load capacity due to deform bar effect and transferring high tensile stress at high strain levels. The increase of AFRP ratio within each group led to more load carrying capacity of T-beams. Specimens with $\rho < \rho_b$ ratio of AFRP were compared when the strength changes from 60 to 80MPa and from 80 to 100MPa. The enhancements in ultimate load capacity were 91.73% and 45.03% respectively. For $\rho_b < \rho < 1.4\rho_b$ The enhancements were 33.54% and 38.80%, and for $\rho > 1.4\rho_b$ were 32.57% and 33.49% respectively. Analytical and experimental beam capacity vs. reinforcement ratio for groups 1, 2, 3 are shown in Fig.14, 15, 16. However, the overall trend of the ANSYS response is compared to experimental results.

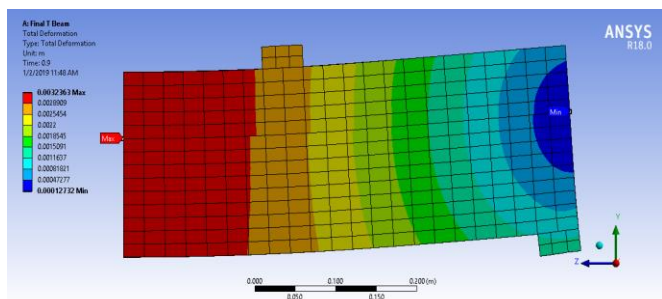


Figure 10: Deflected beam shape for beam sample by ANSYS

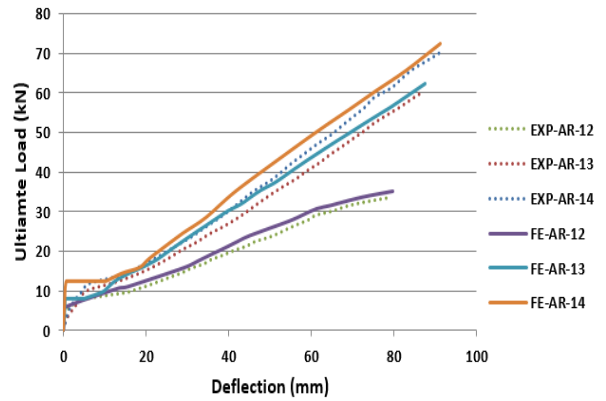


Figure 11: FE model vs experimental load-deflection curve for 60MPa strength group

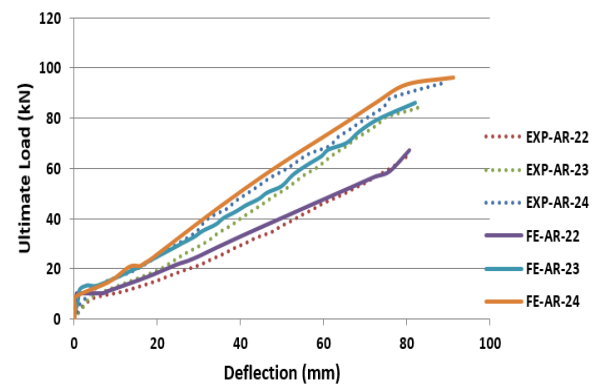


Figure 12: FE model vs experimental load-deflection curve for 80MPa strength group

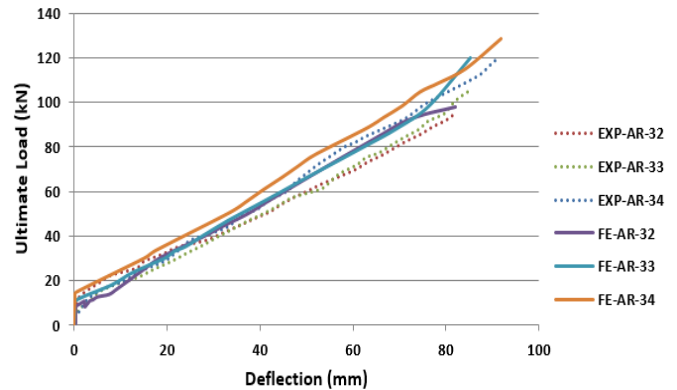


Figure 13: FE model vs experimental load-deflection curve for 100MPa strength group

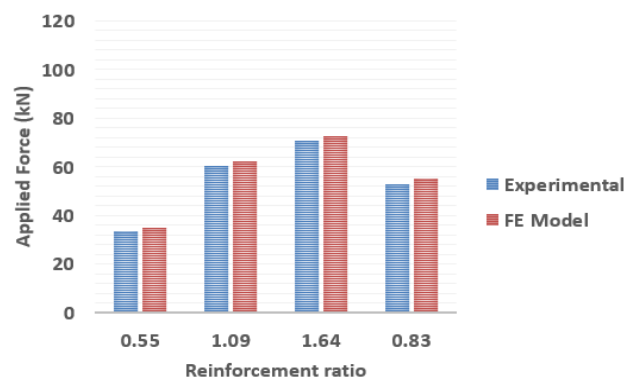


Figure 14: Analytical and experimental beam capacity vs Reinforcement Ratio for Group-3 ($f_c=60\text{MPa}$)

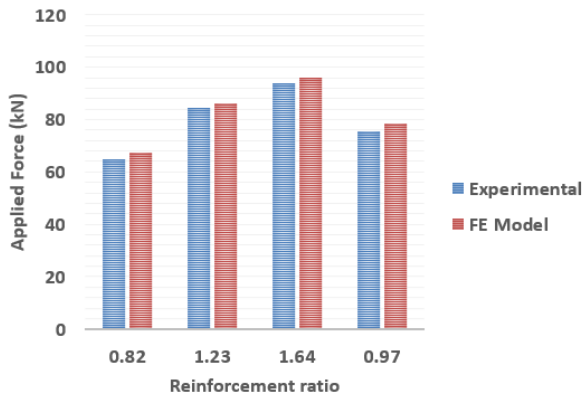


Figure 15: FE and experimental beam capacity vs Reinforcement Ratio for Group-2 ($f_c=80\text{MPa}$)

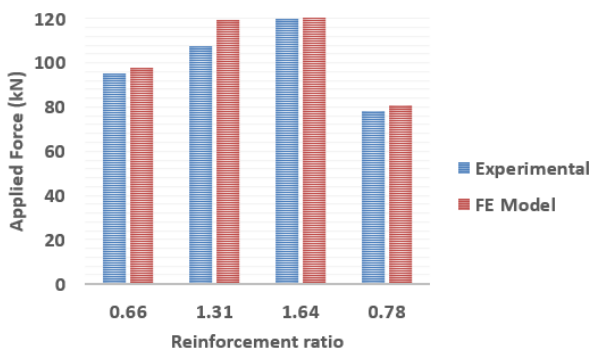


Figure 16: Analytical and experimental beam capacity vs Reinforcement Ratio for Goup-3 ($f_c=100\text{MPa}$)

5. INFLUENCES OF MAJOR PARAMETERS

The aforementioned beam test results were used to investigate the reasons behind the weak representation of design equations for predicting the beam capacity of the reinforced concrete T-beams reinforced with different type bars. To do this, table (6) were prepared showing finite element and experimental crack load ratio and finite element and experimental ultimate (failure) load ratio. And accordingly, it is seen that the crack loads for finite element is so close to 1 and for the ultimate load they are more than 1. This is the indication of accuracy of Finite element models so the load capacity pattern is too close.

Table (6) FE and experimental P_{cr} and P_u load ratio

Sp.No	G.No.	Samples	SCC strength f_c (MPa)	Finite Element First Crack load kN	Experimental First Crack load kN	Pcr FE/Pcr Exp	Finite Element Pu load kN	Experimental Pu load kN	Pu FE/Pu Exp
1	G1	TS-11	60	19.66	21.07	0.933	55.3	52.67	1.050
2		TA-12		6.55	7	0.936	35.1	33.6	1.045
3		TA-13		8.14	8.64	0.942	62.3	60.45	1.031
4		TA-14		9.23	9.82	0.940	72.5	70.7	1.025
5	G2	TS-21	80	20.03	22.63	0.883	78.3	75.64	1.035
6		TA-22		4.12	4.76	0.866	67.3	65.03	1.035
7		TA-23		6.22	6.86	0.907	86.2	84.38	1.022
8		TA-24		9.16	10.16	0.902	96.12	94	1.023
9	G3	TS-31	100	22.12	23.47	0.942	80.71	78.25	1.031
10		TA-32		7.89	8.08	0.976	97.61	95.35	1.024
11		TA-33		8.99	9.13	0.985	119.65	107.57	1.112
12		TA-34		9.07	9.37	0.968	128.32	119.93	1.070

6. CONCLUSION

1-The FE model ultimate load capacity shows slight increase in deflection with respect to the experimental data for all strengths and AFRP ratios. The T-beams reinforced with steel bars show very small deflection compared with AFRP reinforced beams. This is an indication of agreement of the constructed model with the experimental beams. The number of cracks were reduced in all FE models.

2- An increase of AFRP ratio within each group led to more load carrying capacity of T-beams. For $\rho < \rho_b$ the enhancements in ultimate load capacity were 91.73% and 45.03% for (TA-13 and TA-14) respectively over (TA-12). For $\rho_b < \rho < 1.4\rho_b$ the enhancements were 33.54% and 38.80% for (TA-23 and TA-24) respectively over (TA-22), while, it was 32.57% and 33.49% for (TA-33 and TA-34) respectively over (TA-32) for $\rho > 1.4\rho_b$.

3- The steel reinforced beam differs by 57.54%, 16.34%, and -17.31% than aramid reinforced beams for same group of concrete strength in term of final deflection, in which they had balanced reinforcement ratio.

4- The final crack spacing was smaller than experimental samples (which is mean higher number of cracks), taking concrete element (solid65) to be homogenous isotropic material in FE model make the occurrence of first crack be less in number and crack opening less than experimental for the three ratios respectively.

5- The ultimate load capacity of the steel reinforced beam differs by 57.54%, 16.34%, and 17.31% than aramid reinforced beams for same group of concrete strength. These ratios are seen to be more than the experimental data by 0.84%, 1.01%, and 0.65% respectively, this increase in results occurred because that the concrete was taken as homogenous material, so more interlocking between the meshes and higher results is found.

6- For steel reinforced beams of 60MPa and 80MPa strength, ultimate load capacity increases by 41.60%, while for 80MPa and 100MPa strength groups, ultimate load capacity increase by 3.07% showing that the effect of strength change is more in low strengths. These ratios coincide with those of the experimental data.

6- The predicted load of ANSYS model versus the experimental beam data shows a convergence to be ranged from 97-99% for small reinforcement

ratios $\rho < \rho_b$ to $\rho_b < \rho < 1.4\rho_b$ and 90% for larger ratios ($\rho_b < \rho < 1.4\rho_b$ to $\rho > 1.4\rho_b$), this is thereby an indication of perfect calibration of FEM model to perform the simulations close to reality.

7- The models were stiffer than the experimental beams. This came from the non-consideration of the micro-cracks in concrete (because of drying shrinkage), the bond slip of the reinforcement and the assumed perfect bond between the concrete and the reinforcement bar in the FE model, which may not be true for actual beams, and the first cracking loads obtained from the ANSYS-FEM being lower than those from the experimental results in the pre-cracking stages.

8- Analytical and experimental beam capacity vs. reinforcement ratio relations are plotted for all groups. Noting that the overall trend of the ANSYS response is conservative when applied on SCC AFRP reinforced beams compared to experimental data.

Reference

- ABDULLAH A. H., ABDUL KADIR M.R. (2016), Reinforcement for Strengthening Reinforced Concrete Beams-Overview, ZANCO Journal of Pure and Applied Sciences, 28(2), 178-200.
- ACI 440.1R-06. (2006). ACI Committee 440 Guide for the Design and Construction of Concrete Reinforced with FRP Bars, American Concrete Institute, Farmington Hills, Michigan.
- ACI 2013b. CT-13. (2013). ACI Concrete Terminology. ACI STANDARD.
- ANSYS, (2018). ANSYS User's Manual Revision 5.5. Canonsburg, Pennsylvania: ANSYS, Inc.
- BUYUKKARAGOZ, A., KALKAN, I., & LEE, J. H. (2013). A Numerical Study of the Flexural Behavior of Concrete Beams Reinforced with AFRP Bars. Strength of Materials journal, 45(6), 716–729.
- GUOWEI, N., BO, L., XIAO L., & WENSHANG, Y. (2011). Experimental Study on Concrete T-Beams Strengthened with Carbon Fiber Reinforced Polymer (CFRP) Sheets on Three Sides. Systems Engineering Procedia, 1, 69–73.
- KAMAL, H. K., PATRICK, P., AND STEPHAN T. (2001). Structural Performance and In-Place Properties of Self-Consolidating Concrete Used for Casting Highly Reinforced Columns. Materials Journal, 98(5), 371-378.
- NABIL, G., ASCE, M., KENICHI, U., PRINCE, B., AND MENA B. (2013). Flexural Behavior of a Carbon Fiber-Reinforced Polymer Prestressed Decked Bulb T-Beam Bridge System. Journal of Composites for Construction. 17(4).
- OFONIME, A. H., & NDIFREKE, E. U. (2016). Effect of Flange Width on Flexural Behavior of Reinforced Concrete T-Beam. Civil and Environmental Research, 8(8).

- ROLLAND, A., CHATAIGNER, S., BENZARTI, K., QUIERTANT, M., ARGOUL, P., & PAUL, J-M. (2014). Mechanical behaviour of aramid fiber reinforced polymer (AFRP) rebar/concrete interfaces. Transport Research Arena, Paris.
- SRINIVASAN, R. & SATHIYA K. (2010). Flexural behavior of reinforced concrete Beams using finite element analysis (elastic Analysis). Buletin of the political institute in Iași. Technical university "gheorghe asachi" iasi. Tom lvi (Ix), fasc. 4.
- SUBRAMANI, T., MOHAMMED ALI, A., KARTHIKEYAN, R., PANNER SELVAN, E., & PERIYASAMY, K. (2017). Analytical Study Of T-Beam Using ANSYS. International Journal of Emerging Trends & Technology in Computer Science. 6(3).
- YASEEN, S.A. (2020). Flexural Behavior of Self Compacting Concrete T-Beams Reinforced With ARFP. ZANCO Journal of Pure and Applied Sciences, 32(3).
- YASSER S. (2012). Structural performance of Self-Consolidating Concrete used in reinforced concrete beams. KSCE Journal of Civil Engineering, 16(4), 618–626.